

Preparation of highly visible-light active N-doped TiO₂ photocatalyst†

Guidong Yang,^{ab} Zheng Jiang,^b Huahong Shi,^b Tiancun Xiao^{*b} and Zifeng Yan^{*a}

Received 10th February 2010, Accepted 5th May 2010

First published as an Advance Article on the web 24th May 2010

DOI: 10.1039/c0jm00376j

A series of N-doped anatase TiO₂ samples have been prepared using a solvothermal method in an organic amine/ethanol–water reaction system. The effects of different starting N : Ti atomic ratios on the catalysts structure, surface property and catalytic activity have been investigated. The photocatalytic activity and stability of the N-doped TiO₂ samples were evaluated through using the decomposition of Methylene blue (MB) and Methyl orange (MO) as model reaction under visible light irradiation. Characterization results show that the nitrogen dopant has a significant effect on the crystallite size and optical absorption of TiO₂. It was found that the N-doped TiO₂ catalysts have enhanced absorption in the visible light region, and exhibit higher activity for photocatalytic degradation of model dyes (*e.g.* MB and MO). The catalyst with the highest performance was the one prepared using N : Ti molar ratio of 1.0. Electron paramagnetic resonance (EPR) measurement suggests the materials contain Ti³⁺ ions, with both the degree of N doping and oxygen vacancies make contributions to the visible light absorption of TON. The presence of superoxide radicals (O^{•−}) and hydroxyl radicals (OH) on the surface of TON were found to be responsible for MB and MO solution decoloration under visible light. Based on the results of the present study, a visible light induced photocatalytic mechanism has been proposed for N-doped anatase TiO₂.

1. Introduction

As a well-known photocatalyst, TiO₂ has attracted lots of interest over the past decades due to its special optoelectronic and physiochemical properties. Some potential applications of TiO₂ have been developed including solar energy conversion^{1,2} and environmental purification.^{3–5} However, the main drawback is that TiO₂ photocatalysts may only be excited by ultraviolet (UV) light (wavelength $\lambda < 388$ nm) due to their wide band gap. Therefore, the overall efficiency of TiO₂ remains too low under natural sunlight irradiation, as UV only accounts for about 4% of the incoming solar energy on the Earth's surface.⁶ With the purpose of utilization a wider solar spectrum in the application of TiO₂, considerable efforts have been devoted to the preparation and characterization of visible-light-active titanium dioxide (TiO₂) materials doped with nonmetal impurities,^{7–11} and this strategy is regarded to be one of the most promising techniques for the harvest of sunlight by TiO₂ photocatalysts.

Since the discovery of N-doped TiO₂ with a visible light absorption by Asahi *et al.*,¹² great attention has been given to modifying the electronic band gap of TiO₂ by nitrogen doping.^{13–15} Compared to the other nonmetal elemental doping, N-doped TiO₂ materials exhibit a significant photocatalytic activity and strong absorption in the various reactions performed under visible light irradiation.

Recently, a large number of studies have focused on the preparation of powder and film N-doped TiO₂ by a variety of synthesis routes. Generally, the synthetic methodology used to prepare N-doped TiO₂ can be classified into two groups; physical methods such as ion implantation,^{16,17} sputtering¹⁸ and ball milling,¹⁹ and chemical methods such as hydrolyzation of titanium alkoxides by sol–gel method,^{14,20,21} direct hydrolysis of organic or inorganic salt under hydrothermal¹⁵ or solvothermal²² conditions and the oxidation of titanium nitride.^{23,24} Numerous studies have shown that nitrogen species could be incorporated into the anatase TiO₂ crystalline structure by the above-mentioned methods, although these different synthetic procedures can lead to doped TiO₂ with somewhat different photocatalytic properties.

It is well-accepted that N doping can cause the red-shift absorption threshold of TiO₂, but the doping mechanism is still debated. Most authors claim that the substitutional doped N for O in anatase TiO₂ yields a narrowing of band gap driven by mixing N 2p states with O 2p states.^{12,25} It is believed that an N atom is doped into the TiO₂ anatase lattice and forms a donor state just above the top of the valence band. This process leads to the narrowing of the band gap of TiO₂ and the creation of oxygen vacancy, both of which enhance visible light absorbance.^{26,27} More recently, Livraghi *et al.*²⁸ found that N-doped titanium dioxide contains single atom nitrogen impurities forming N_b centers, which are responsible for the visible light absorption, with the promotion of an electron from the band gap localized (N donor) states to the conduction band or to surface-absorbed electron scavengers. A better understanding of the visible light induced mechanism will lead to the development of an appropriate preparation method for the doped photocatalyst and thus it is useful to identify the optically active species present and to rationalize their roles.

^aState Key Laboratory for Heavy Oil Processing, China University of Petroleum, Qingdao, 266555, China. E-mail: zfyancat@upc.edu.cn; Fax: +86 532 86981295; Tel: +86 532 86981296

^bDepartment of Chemistry, Inorganic Chemistry Laboratory, University of Oxford, Oxford, OX1 3QR, U.K. E-mail: Xiao.tiancun@chem.ox.ac.uk; Fax: +44 1865 272690; Tel: +44 1865 272660

† Electronic supplementary information (ESI) available: Fig. S1 and S2. See DOI: 10.1039/c0jm00376j

Here, we developed a simple preparative method for N-doped TiO₂ materials at low temperature whereby an ethanol–water solvothermal method with organic ammonia (ethylenediamine) as the nitrogen source to enhance nitrogen incorporation into titanium dioxide is used. The degrees of nitrogen doping and visible light active mechanism have also been studied. The prepared N-doped materials exhibit a significant increased absorption of visible light and substantial photocatalytic activity.

2. Experimental section

2.1 Materials

Analytical grade tetrabutyl orthotitanate (C₁₆H₃₆O₄Ti, >97% Fluka chemicals) and ethylenediamine (99% Alfa Aesar) were utilized. All chemical reagents were used as received without further purification.

2.2 Preparation of photocatalyst

A series of N-doped TiO₂ photocatalysts with different nominal nitrogen doping level in the range of 0.5–2.0 (molar ratio of nitrogen to titanium) were prepared by solvothermal method as described in our previous work.²⁹ In a typical procedure, tetrabutyl orthotitanate (C₁₆H₃₆O₄Ti, 0.01 mol) and ethanol (30 ml) were mixed together and stirred for 30 min, and then 1.0 ml of acetic acid was added. A specific amount of ethylenediamine was then added dropwise whilst stirring with the concentration of nitrogen doping chemical varying from 0.005 mol to 0.02 mol. The details of the addition are described as following, 1.0 ml of deionized water was added into the mixture, and stirring continued for a further 30 min. Next, the mixed solution was transferred into a Teflon-lined stainless steel autoclave and kept at 120 °C for 20 h. After reaction, the autoclave was removed from the oven and cooled to room temperature. The white doped TiO₂ powder was obtained by filtrating and washing with deionized water and ethanol several times, and then dried at 80 °C overnight. The resultant pale-yellow material was then annealed at 450 °C for 3 h in air to prepare the final N-doped TiO₂ samples. The obtained samples with different starting N : Ti molar ratios of 1 : 2, 1 : 1, 3 : 2 and 2 : 1 were named TON-1, TON-2, TON-3, TON-4, respectively. The undoped TiO₂ was prepared by the same approach. The commercial P25 TiO₂ powder was used as a reference without further treatment.

2.3 Characterization

The crystalline structure of the resulting anatase doped TiO₂ were determined by X-ray diffraction using a Philips X'Pert Pro Alpha 1 diffractometer with Cu-K α radiation ($\lambda = 1.5406 \text{ \AA}$) operated at a tube current of 40 mA and a voltage of 45 kV. Data were collected over 2θ values from 20° to 80°, at a scan speed of 1°/min. The average crystal size was calculated using Scherrer equation based on the strongest XRD peak of anatase (101) TiO₂. The UV-vis diffuse reflectance spectra were obtained using a Perkin Elmer Lambda 750S UV/Vis spectrometer equipped with an integrating sphere assembly. The spectra were recorded at room temperature in air from 300 to 700 nm. X-Ray

photoelectron spectroscopy was performed using a Perkin-Elmer RBD upgraded PHI-5000C ESCA system with monochromatic Mg-K α excitation and a charge neutralizer was used to investigate the surface electronic states of the N doped samples. All the bonding energies were calibrated to the C 1s internal standard peak (284.8 eV) of surface carbon. Laser Raman spectra were obtained using a Perkin Elmer 400F Ramanstation Raman spectrometer. Fourier transform infra red (FTIR) spectra were carried out by diffused reflectance using a Bruker Vertex-70. The BET specific surface area and pore volume analysis of the N-doped TiO₂ were determined using a N₂ physisorption technique, the sample was degassed at 180 °C overnight before the actual measurement. The electron paramagnetic resonance (EPR) spectra were recorded on an X-band Bruker EMX spectrometer operating at 100 KHz field modulation and 1 mW microwave power and equipped with a high-sensitivity cavity (ER 4119HS). The g values were determined using a DPPH standard.

2.4 Photocatalytic activity tests

Methylene blue (MB) and Methyl orange (MO) are two common dyes, extensively used in various industrial applications. Therefore, many studies have chosen them as model pollutant to evaluate the photocatalytic degradation over N-doped titania catalysts.^{28–31} It should be noted that the Methylene blue itself is a photosensitive dye which would gradually degrade under light irradiation even without the presence of the photocatalyst. In contrast, Methyl orange is a very stable dye. To confirm the catalyst performance, the degradation of the both dyes was tested over the as-prepared catalyst samples in this work. The degradation of model dyes (MO and MB) was carried out in a self-designed 200 ml reactor fitted with a circulating water cooling system to maintain constant temperature. A xenon lamp (Trustech, PLS-SXE300) was used as the visible light source, with all the UV light below 420 nm being removed with a glass filter. The distance between the strip lamp and fluid level was kept as 15 cm. The initial concentration of model dye solution was 10 mg L⁻¹. 100 mg of the as-prepared N-doped TiO₂ catalyst and 100 ml of aqueous solution of model dye were added into the reaction system. Before illumination, the suspension was magnetic stirred for 2 h in the dark to ensure the mixture had reached adsorption equilibrium. During the photoreaction process, 3 ml of the solution was removed in a constant time, the photocatalyst separated from the solution by centrifugation and the concentration of the remaining clear liquid tested by UV-visible spectroscopy. No oxygen was bubbled into the suspension during the photoreaction.

3. Results and discussion

Fig. 1 shows the X-ray diffraction patterns of N-doped TiO₂ prepared with varying molar ratios of nitrogen to titanium, including data for undoped P25, used here as a reference, which has a mixture of anatase and rutile phases. All the as-prepared TiO₂ materials have single phase, crystalline, anatase TiO₂ (JCPDS no. 71-1168) except TON-3 sample, which is poorly crystalline anatase together with a small amount of rutile TiO₂. No new diffraction peaks are observed in the N containing phase.

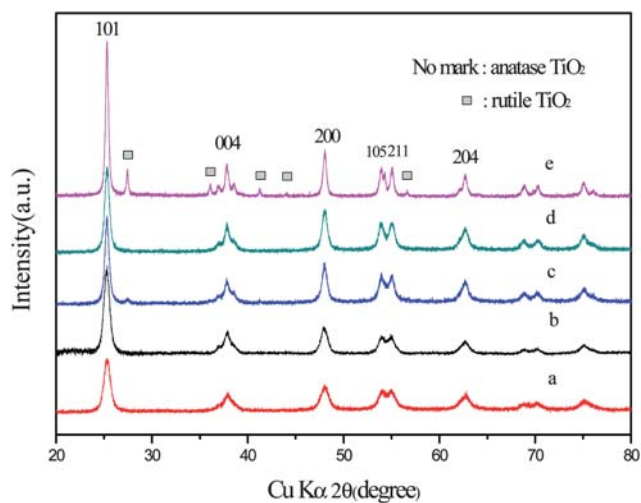


Fig. 1 X-Ray diffraction data for N-doped TiO_2 samples with different starting N: TiO_2 molar ratio: (a) TON-1; (b) TON-2; (c) TON-3; (d) TON-4; (e) P25.

Table 1 Crystal size and phase composition of N-doped TiO_2 with different starting N: TiO_2 molar ratio

Samples	N: TiO_2 molar ratio	Phase composition	Average crystallite size/nm
TON-1	1/2	Anatase	8.8
TON-2	1/1	Anatase	9.6
TON-3	3/2	Anatase, Rutile	15.1
TON-4	2/1	Anatase	16.3
P25 (reference)	—	Anatase, Rutile	33.0

Table 1 lists the crystal size of N-doped TiO_2 with different starting N: TiO_2 molar ratio, which were calculated by Scherrer equation. It is well known that particle sizes play a vital role in photocatalytic activity since smaller crystals offer greater surface area to volume ratios and thus induce better surface absorbability of hydroxyl/water, which in-turn acts as an active oxidizer in the photocatalytic reaction.¹⁴ It can be seen that the crystallite sizes of N-doped TiO_2 calculated using Debye-Scherrer equation from the diffraction data is smaller than that of the reference P25 catalyst. In addition, the increase of nominal nitrogen content leads to an increase of the average crystal size of N-doped TiO_2 , from 8.8 nm to 16.3 nm. It can therefore be concluded that the level of nitrogen doping has a significant effect on the particle size of TiO_2 grown during the doping process.

Fig. 2 shows the corresponding UV-vis diffuse reflectance spectra of pure TiO_2 (P25 catalyst) and N-doped TiO_2 prepared with varying molar ratios of nitrogen to titanium. The doped samples have an apparent adsorption in the visible region between 400 and 500 nm (the samples are bright yellow in color). Interestingly, a monotonic increase in the UV-vis DRS spectra of N-doped TiO_2 samples was detected, indicating that the absorbance threshold of N-doped TiO_2 shows an increasing red-shift with increasing nitrogen content. At lower N: TiO_2 molar ratios (1 : 2, 1 : 1 and 3 : 2), the optical absorption edge of TiO_2 was only 460 nm, whereas when the N: TiO_2 molar ratio is increased to 2, a shift in the optical absorption edge of TiO_2 into the visible

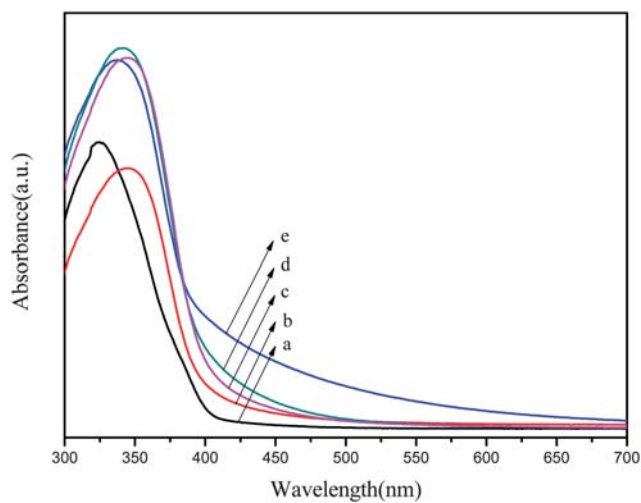


Fig. 2 UV-vis diffuse reflectance spectra of pure TiO_2 and N-doped TiO_2 with different doping level: (a) pure TiO_2 (P25); (b) TON-1; (c) TON-2; (d) TON-3; (e) TON-4.

light region, at 650 nm, was observed. Thus, the degree of nitrogen doping strongly affects the visible light absorption of TiO_2 , leading to the monotonic increase in optical absorption with increasing N: TiO_2 molar ratio. Compared to doped TiO_2 , P25 has almost no visible absorption, which suggests that the increased absorption of doped TiO_2 can be related to the presence of nitrogen species in the samples.

In Fig. 3a, we show the whole XPS survey spectra for TON-2 calcined at 450 °C for 3 h, which indicated that it contained predominantly Ti, O, N, and C elements. Among these elements, the contaminant C1s peak is located at 285.7 eV, which was mainly ascribed to remnant organic precursors not completely removed during the annealing treatment. Moreover, part of the adventitious carbon may also cause the presence of C element. The N1s XPS spectra for TON-2 is shown in Fig. 3b, the broad peak can be fitted by three peaks at 406.0, 401.6 and 397.5 eV, suggesting three independent environments for N within TON-2. The high binding energy (BE) of around 406.0 eV can be assigned to nitrogen species bound to various surface oxygen sites (such as NO or NO_2 molecules).^{32,33} The N1s peak at 401.6 eV can be attributed to the nitrogen in the form of an Ti–N–O linkage, and the low bonding energy component located at 397.5 is generally known as the N atom replacing the oxygen atoms in the TiO_2 crystal lattice to form an N–Ti–N bond.^{34,35} The relative atomic concentrations of N in the TON-2 sample was found to be 5.2 at.% based on the XPS data.

Fig. 3c shows a Ti 2p XPS spectra of TON-2. Here, two peaks were observed at 464.8 and 459.1 eV, and were assigned to Ti 2p_{1/2} and Ti 2p_{3/2}, respectively. These data agree well with previously reported XPS data for N-doped TiO_2 ^{34–36} and arise from the presence of Ti^{4+} in pure anatase titanium. Besides, the trace of Ti^{3+} was not observed by XPS, although it was observed by EPR spectroscopy (see Fig. 6). This is thought to be due to either the low resolution of the XPS, which was unable to detect minor changes to TiO_2 or because the Ti^{3+} species exist in the subsurface or bulk, which is inaccessible by XPS. Fig. 3d shows an O 1s XPS spectra of TON-2, with the asymmetric O1s peak

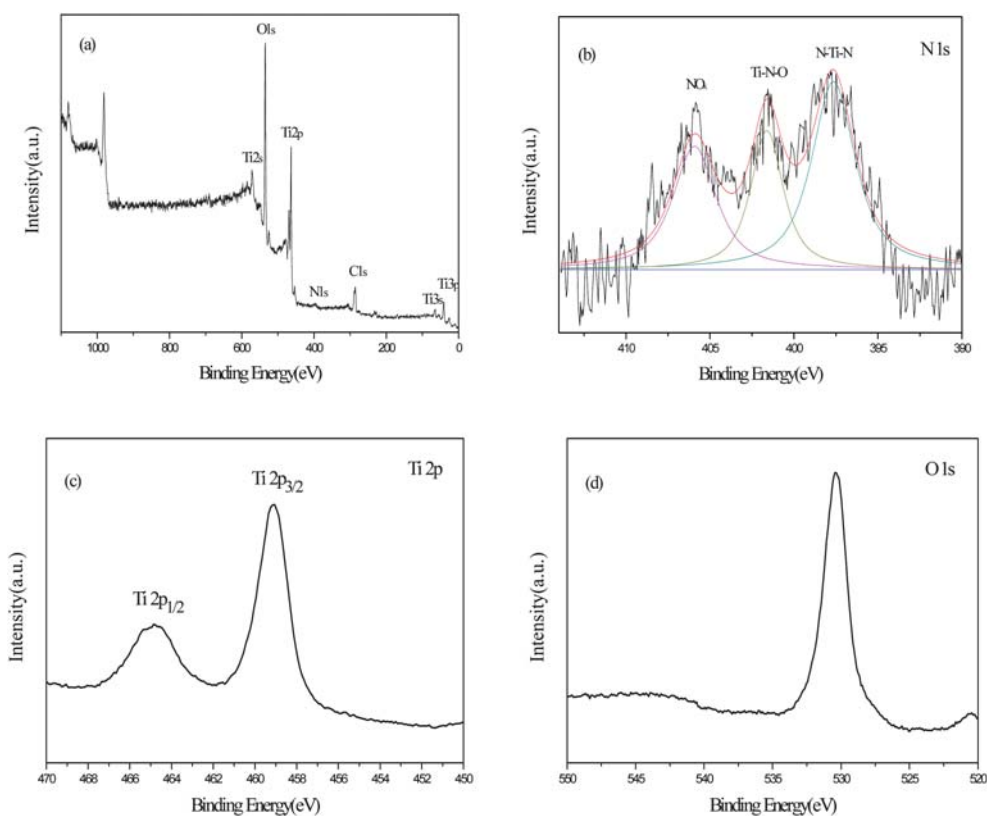


Fig. 3 X-Ray photoelectron spectroscopy spectra of TON-2: (a) the survey spectra of N-doped TiO₂ (b) N1s XPS spectra; (c) Ti2p XPS spectra; (d) O1s XPS spectra.

located at 530.3 eV, which corresponds to lattice oxygen of TiO₂, and is consistent with previous studies of TiO₂.³⁴

Fig. 4 displays the FT-IR spectra of N-doped TiO₂ prepared by solvothermal approach with varying molar ratios of nitrogen to titanium. All the samples present similar spectra, with the strong band located at ~700 cm⁻¹ attributed to Ti–O stretching and Ti–O–Ti bridging stretching modes.³⁷ The peak at around ~1630 cm⁻¹ corresponds to bending vibrations of O–H and N–H.^{38,39} The broad band at 3400 cm⁻¹ was observed in the spectra of doped samples, which can be ascribed to surface hydroxyl groups and absorbed water molecules.^{14,40} The right

spectra of Fig. 4 shows the localized profile of the FT-IR spectra range from 1000 cm⁻¹ to 1550 cm⁻¹. The bands at around 1474 cm⁻¹, 1250 cm⁻¹ and 1080 cm⁻¹ are attributed to the vibrations of the Ti–N bond,⁴¹ while the band at 1390 cm⁻¹ can be ascribed to the vibration of surface-absorbed NO₃⁻¹. The appearance of the N–Ti bond in the samples with varying N:TiO₂ ratios suggests that the N species have been incorporated into the TiO₂ lattice. This finding is in accordance with the XPS result previously discussed.

Fig. 5 shows the Raman spectra of the N-doped TiO₂ powders with varying N : TiO₂ molar ratios. According to the previously

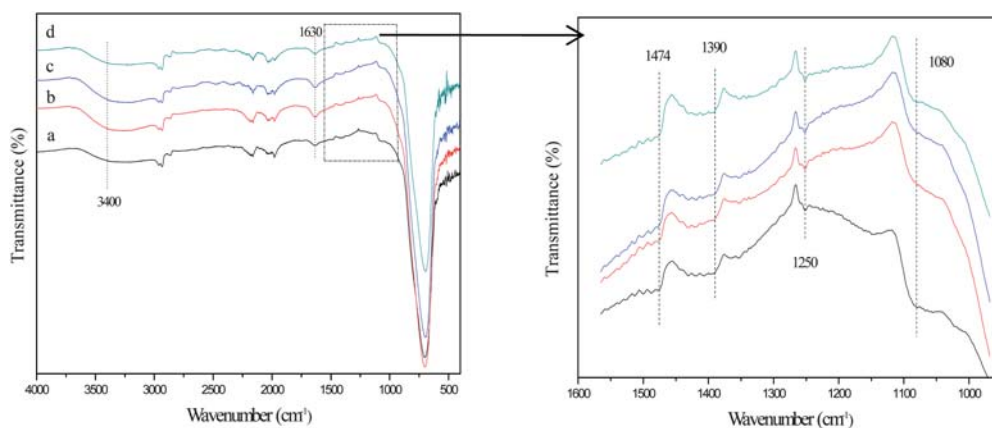


Fig. 4 FT-IR spectra of N-doped TiO₂ with different starting N : TiO₂ molar ratio: (a) TON-1; (b) TON-2; (c) TON-3; (d) TON-4. The right figure shows the enlarged localized profiles of N-doped TiO₂.

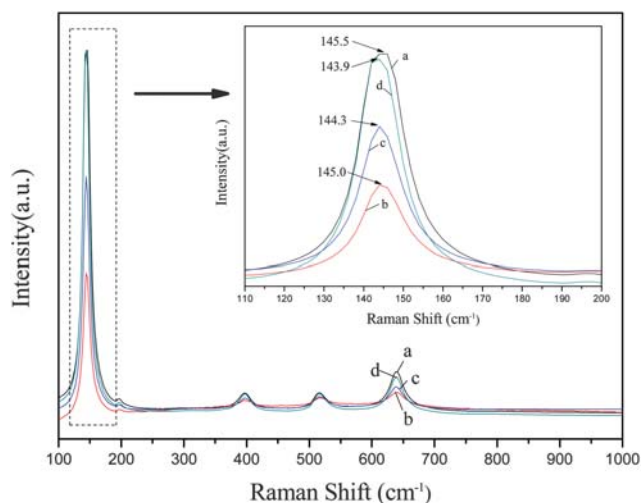


Fig. 5 Raman spectra of N-doped TiO₂ with different starting N : TiO₂ molar ratio: (a) TON-1; (b) TON-2; (c) TON-3; (d) TON-4. The inset is the enlarged localized profiles of N-doped TiO₂.

reported data,^{42,43} the anatase phase of TiO₂ has six Raman bands at 144 cm⁻¹(E_g), 197 cm⁻¹(E_g), 399 cm⁻¹(B_{1g}), 513 cm⁻¹(A_{1g}), 519 cm⁻¹(B_{1g}) and 639 cm⁻¹(E_g), and the rutile phase has four Raman bands at 143 cm⁻¹(B_{1g}), 447 cm⁻¹(E_g), 612 cm⁻¹(A_{1g}), and 826 cm⁻¹(B_{2g}). All our samples present Raman spectra the same as the pure anatase phase, with no peaks due to the rutile phase. The inset shows the enlarged localized profiles of

N-doped TiO₂. Comparing the four Raman spectra, it is clear that the predominate Raman bands shift towards lower wavenumber from TON-1, TON-2, TON-3, to TON-4, indicating that the particle size of the doped TiO₂ increases with increasing N doping. This observation is in good agreement with those from the X-ray diffraction data.^{44,45}

Previous EPR studies suggest the presence of various paramagnetic species in the bulk or the surface of N-doped TiO₂, including the formation of \dot{O}^- radical and Ti³⁺ ions during the N-doping process.^{14,30,46} Here, CW EPR spectroscopy was used to examine the paramagnetic species of N-TiO₂ nanoparticles. Fig. 6a shows the EPR spectra of TON-3 recorded at room-temperature. The resonance at $g = 2.004$, is the most prominent electron signal and is characteristic of paramagnetic materials containing "F-centers" or oxygen vacancies.^{46,47} Fig. 6b is corresponding to the EPR spectra of TON-1 recorded at room-temperature. The resonances at g values of less than 2.0 are known to be due to photogenerated electrons stabilized in Ti cations located at crystallization defects.⁴⁷⁻⁵⁰ These trapped electrons could reduce Ti⁴⁺, leading to the formation of Ti³⁺ paramagnetic species according to the following equation $e^- + TiO_2(Ti^{4+}) \rightarrow TiO_2(Ti^{3+})$, which has been extensively reported,⁴⁷⁻⁵⁰ or alternatively could reduce surface-absorbed oxygen on TiO₂ active sites, to form superoxide ions (O₂⁻). Signals with g values in the range of 2.0 to 2.08 can be attributed to photogenerated holes trapped by subsurface lattice oxygens.⁴⁷⁻⁵⁰ It is known that the holes are localized on the oxygen vacancies, reacting with the O²⁻ and OH⁻ to form \dot{O}^- and OH radicals on the catalyst surface,

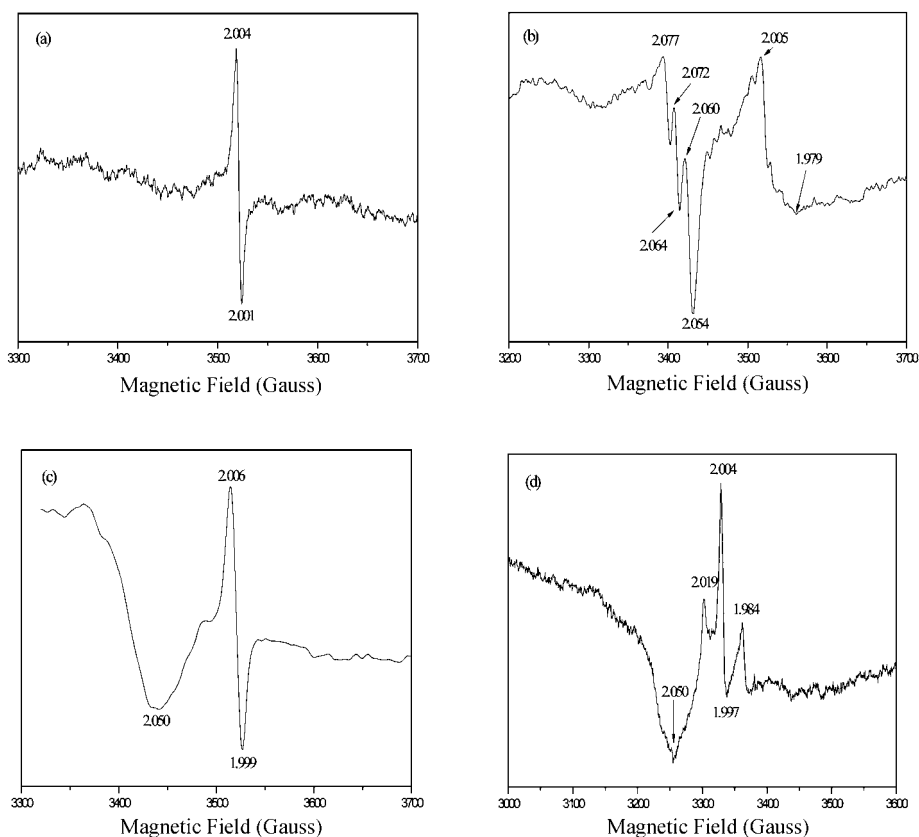


Fig. 6 EPR spectra of N-doped TiO₂ samples. (a) TON-3; (b) TON-1; (c) TON-2, these three samples recorded at room-temperature; (d) TON-2 recorded at 100 K. Instrument setting: microwave power, 10 dB; microwave frequency, 9.51 GHz; modulation amplitude, 1 G at 100 KHz.

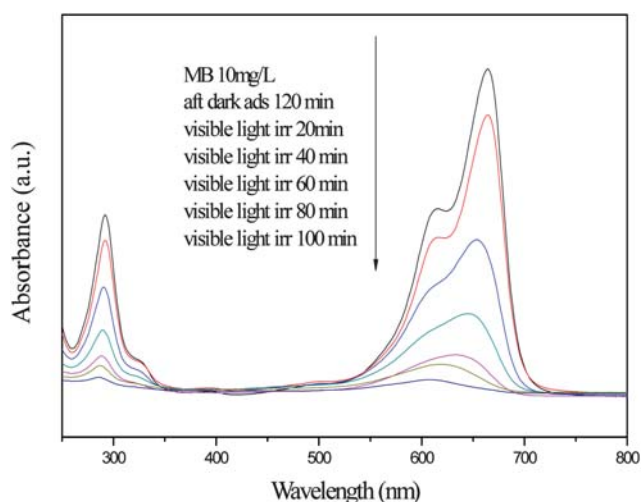


Fig. 7 UV-vis diffuse reflectance spectra of MB solution before and after visible light irradiation ($\lambda > 420$ nm) for different exposure times in the presence of TON-2.

both of which are responsible for the oxidative decomposition of organic pollutants. From the area of the integrated signals, it revealed that a high amount of \dot{O}^- radical existing on the surface of doped materials, which could facilitate photocatalysis. As shown in Fig. 6c, the signals of trapped hole and electron were also observed, suggesting the presence of superoxide radical and Ti^{3+} ions in the TON-2 sample.

As demonstrated previously,⁵⁰ the strategy of using lower temperature to reduce the rate of electron-hole pair recombination enables EPR examination and characterization of these paramagnetic species. Therefore, the paramagnetic properties of the TON-2 sample (which showed both trapped hole and electron signals) were analyzed by EPR spectroscopy at 100 K. The corresponding EPR spectra is shown in Fig. 6d, in comparison with the EPR signal of TON-2 recorded at room temperature (Fig. 6c), we observe two additional peaks at $g = 2.019$ and 1.984 , which suggested an increase in the concentration of trapped electron and holes at lower temperature. In addition, the g value of lattice-trapped electrons changed from $g = 1.999$ at room-temperature to $g = 1.997$ at 100 K, and that of trapped hole changed from $g = 2.006$ at room-temperature to $g = 2.004$ at 100 K accompanied by a narrowing of the signal which is indicative of small changes in structure.

Methylene blue (MB) was used as the model organic pollutant to evaluate the photocatalytic activity of the N-doped TiO_2 nanomaterials. Fig. 7 shows the UV-vis diffuse reflectance spectra of MB solution before and after visible light irradiation ($\lambda > 420$ nm) for different exposure time in the presence of TON-2. The characteristic absorption bands of MB solution at 664 nm were significantly decreased in intensity with increasing irradiation time. The absorbance of this peak approaches to 0 and the eventual position moves to ~ 600 nm after illumination for 100 min, indicating the solution has been completely decolorized with a $1.0 g L^{-1}$ TON-2 suspension.

In Fig. 8, we show the visible light-induced photocatalytic activity for the degradation of Methylene blue (MB) over N-doped TiO_2 photocatalyst synthesized with different doping

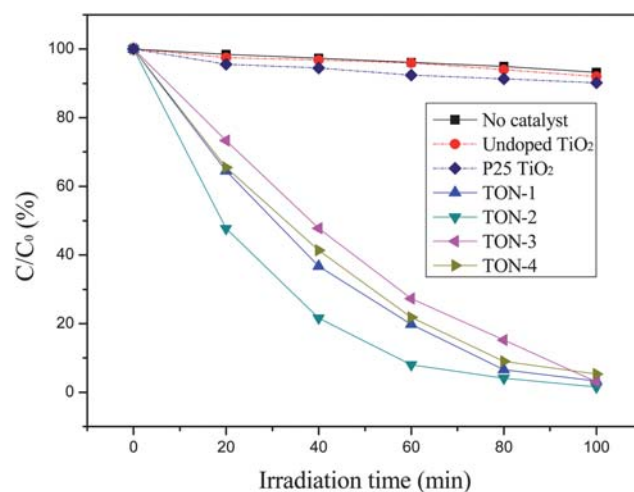


Fig. 8 Photocatalytic degradation of Methylene Blue (MB) over TiO_2 samples with varying N : TiO_2 molar ratio under visible light irradiation ($\lambda > 420$ nm). Reaction conditions: $C_0 = 10$ ppm, Catalyst loading: $1 g L^{-1}$.

levels. It can be seen the direct illumination without catalyst could lead to only about 7% decomposition of MB solution within 100 min, which accounts for the photosensitized capability of MB molecules. The undoped TiO_2 and P25 samples are essentially inactive since they could not be activated by visible light due to their big energy gap (3.2 eV). The photocatalytic activity of N-doped TiO_2 were enhanced greatly under visible light irradiation as compared with the references, suggesting that the N doping level had an obvious influence on the photocatalytic activity of the TiO_2 samples. TON-2 shows the highest photodegradation activity with a MB conversion of 92% after 60 min irradiation, the TON-3 has a lower catalytic performance. The degradation yield of TON-3 is merely 70% in the same irradiation time.

In order to avoid the photosensitized process of MB molecules, the activity of the as-prepared catalysts was also evaluated by photocatalytic degradation of Methyl orange under visible lights irradiation ($\lambda > 420$ nm). Fig. 9 shows the photocatalytic activity of pure titania and N-doped TiO_2 with varying N doping levels. It was seen that the MO solution is very stable and no decomposition in the absence of photocatalyst can be observed at all. As expected, the undoped samples (including commercial P25 TiO_2) show no photocatalytic activity at all under visible light illumination. It is worth mentioning that due to the nitrogen bearing the positive charge is involved in a double bond in the azo chemical structure of MO molecule, it is difficult to photodegrade compared with the MB solution. However, as shown in Fig. 9, the N-doped TiO_2 catalyst samples give greater activity and the MO solution is completely decolorized under visible light irradiation. Similarly, the TON-2 sample shows the highest activity among all the N-doped TiO_2 samples. It is therefore concluded that N-doping is very important to improve the visible light photocatalytic performance, however, there is not directed correlation between the activity and the N-doping content, although the UV-vis spectra showed that the TON-4 prepared with the highest nitrogen content in the starting materials show the strongest absorbance for visible lights (see Fig. 2).

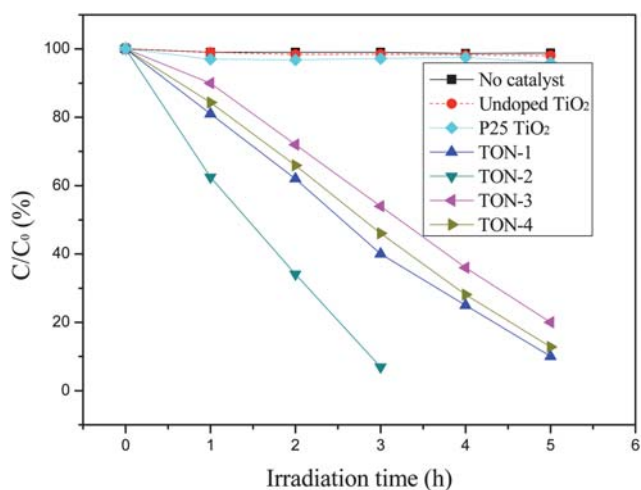


Fig. 9 Photocatalytic degradation of Methyl orange (MO) over TiO_2 samples with varying N : TiO_2 molar ratio under visible light irradiation ($\lambda > 420$ nm). Reaction conditions: $C_0 = 10$ ppm, catalyst loading: 1 g L^{-1} .

As described above, both the degradation of the Methylene blue and Methyl orange over the TON catalysts show similar trends: the undoped TiO_2 samples have little ability to discolor the reaction, and the TiO_2 samples modified with nitrogen display higher activity owing to the spectral response in visible light region. This is due to the N doped into the TiO_2 lattice to form an intermediate energy level, and leading to the narrow band gap of TiO_2 . Among the TON samples, the TON-2 shows the highest catalytic performance, it is thought to result from the synergic effect of the pure anatase phase structure, small crystallite size, high specific surface area ($171.7 \text{ m}^2 \text{ g}^{-1}$), large pore volume ($0.32 \text{ cm}^3 \text{ g}^{-1}$) and higher crystallinity of the sample. It is known that the well crystallized anatase might facilitate the transfer the photoelectrons from bulk to surface and thus inhibit their recombination with the photohole, leading to the enhanced quantum efficiency.

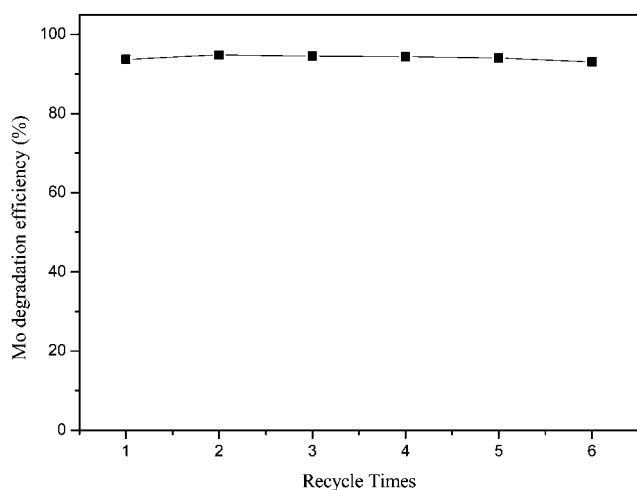


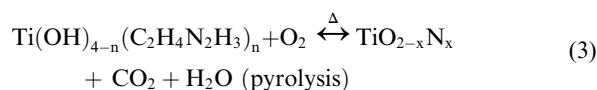
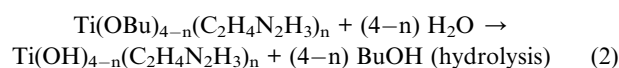
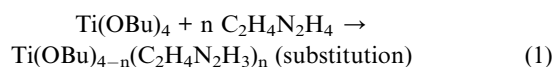
Fig. 10 Recycling testing of the TON-2 sample for photocatalytic degradation of Methyl orange. Reaction conditions: $C_0 = 10$ ppm, catalyst loading: 1 g L^{-1} , reaction time: 3 h.

Besides the highest activity, the TON-2 also shows strong stability and durability during photocatalytic degradation of MO solution. As shown in Fig. 10, after recycling 6 times, the TON-2 sample can still completely degrade the Methyl orange in 3 h, suggesting that TON has a good reusability of the catalytic measurement. It can be seen that the MO degradation efficiencies were rather stable over TON-2 catalysts.

Before running the photocatalytic reaction, we also have carried out an absorption test of N-doped TiO_2 in the dark environment, and the results of dye absorption curve were shown in Fig. S1 and Fig. S2 (ESI[†]). It can be seen that all the N-doped TiO_2 samples exhibit stronger physical absorption of MB solution than that of MO, and both of the mixture have completely reached adsorption equilibrium after two hours.

Formation mechanism of the N-doped TiO_2

We propose the following possible mechanisms for the formation of N-doped TiO_2 (TON) using amine as the nitrogen source in the doping process. At the beginning, the starting solution contained two components: $\text{Ti}(\text{OBu})_4$, and $\text{C}_2\text{H}_4\text{N}_2\text{H}_4$, $\text{Ti}(\text{OBu})_4$ dissolved rapidly in the solvent and reacted with $\text{C}_2\text{H}_4\text{N}_2\text{H}_4$ to generate the substituted $\text{Ti}(\text{OBu})_{4-n}(\text{C}_2\text{H}_4\text{N}_2\text{H}_3)_n$ precursor according to the reaction (1). A small amount of H_2O was added dropwise to controllably hydrolyse Ti-based component into hydrous TiO_2 , this process is represented by reaction (2). After the hydrolysis reaction, the resultant products was annealed at high temperature, eventually forming the N-doped TiO_2 (eqn (3)). Importantly, the presence of the N–Ti bonds in TON was detected by XPS spectra, confirming the N-doping into the TiO_2 crystalline lattice.



Visible light-induced photoactivity in N-doped TiO_2 : a mechanistic view

In this study, we have also attempted to understand the mechanism of visible light-induced photocatalytic activity of the N-doped TiO_2 nanomaterials. There are a large number of reports that have focused on the photocatalytic activity mechanism of N-doped TiO_2 .^{25–28} It is widely accepted that the N incorporation into the crystalline lattice of TiO_2 modifies the electronic band structure of TiO_2 , leading to a new substitution N 2p band formed above O 2p valance band, which narrows the band gap of TiO_2 and shifts optical absorption to the visible light region. Here, we note that the creation of a Ti^{3+} donor band also contribute to photoabsorption in doped TiO_2 . Because electron-hole pairs are generated by excitation under visible light irradiation, these charge carriers rapidly diffuse to the surface of TiO_2 unless they are trapped or recombine. The presence of excess

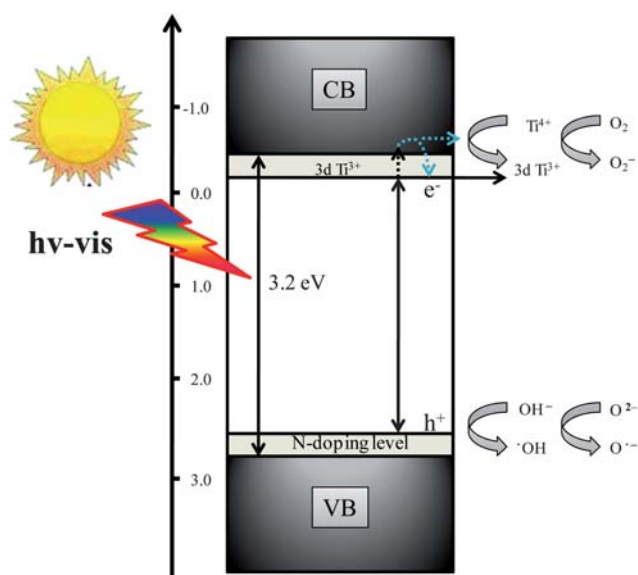


Fig. 11 A possible mechanism of photocatalytic reactions of $\dot{\text{O}}^-$ radical and the schematic band structure of N-doped TiO_2 under visible light irradiation.

electrons can cause reduction of the Ti^{4+} and the generation of Ti^{3+} species in the bulk of anatase polycrystalline TiO_2 samples, with consequent formation of the 3d orbital of the Ti^{3+} ions in the band gap, which is found to be below the bottom of the conduction band (CB). The electrons might be transferred from CB to the new Ti^{3+} states and eventually localized there and this is therefore caused a magnetic resonance detected by EPR experiments.^{51,52} Hence, we believe that both of the N impurity and Ti^{3+} act cooperatively to narrow the band gap of N-doped TiO_2 , resulting in the visible light activity of N-doped TiO_2 . As mentioned above, N doping can also lead to the formation of the oxygen vacancies, which were observed by EPR spectroscopy. These paramagnetic species should also contribute to the visible light response.⁵³ As shown in Fig. 11, the electron transfers directly into the conduction band of TiO_2 , reducing O_2 to form superoxide ions (O_2^-). The hole (h^+) then reacts with OH^- group to produce $\cdot\text{OH}$ radical, which are responsible for the degradation of Methylene blue and Methyl orange under visible light irradiation.

4. Conclusions

We demonstrated a new facile solvothermal method for preparation of high quality N-doped TiO_2 with pure anatase phase using amine as a nitrogen source. By tuning the starting molar ratio of nitrogen to titanium, different doping level samples were obtained, which show a stable and high photocatalytic activity for degradation of model dye (MB and MO) solution under visible light irradiation. Higher N : Ti molar ratios resulted in larger crystal size and stronger visible light absorption, but the photocatalytic activity did not linearly increase with the increasing molar ratio of nitrogen to titanium. The optimum N doping level was found to be N : Ti = 1.0, which gives the highest photocatalytic degradation rate of the dyes. The EPR spectroscopy showed the formation of Ti^{3+} works cooperatively with N doping

and plays an essential role in the absorption of visible light. Additionally, N-doping caused the generation of the oxygen vacancies also makes a contribution to the visible light response of the N-doped TiO_2 materials.

Acknowledgements

Thanks are due to the UK Photocatalysis Network for their kind support. Guidong Yang thanks a scholarship from the China Scholarship Council (CSC).

References

- 1 M. Anpo and M. Takeuchi, *J. Catal.*, 2003, **216**, 505–516.
- 2 J. Tang, J. R. Durrant and D. R. Klug, *J. Am. Chem. Soc.*, 2008, **130**, 13885–13891.
- 3 M. R. Hoffmann, S. T. Martin, W. Choi and D. W. Bahnemann, *Chem. Rev.*, 1995, **95**, 69.
- 4 M. A. Fox and M. T. Dulay, *Chem. Rev.*, 1993, **93**, 341.
- 5 T. Morikawa, T. Ohwaki, K. Suzuki, S. Moribe and S. Tero-Kubota, *Appl. Catal., B*, 2008, **83**, 56–62.
- 6 A. Kudo, K. Omori and H. Kato, *J. Am. Chem. Soc.*, 1999, **121**, 11459.
- 7 X. Chen and C. Burda, *J. Am. Chem. Soc.*, 2008, **130**, 5018.
- 8 J. Xu, J. Li, W. Dai, Y. Cao, G. Li and K. Fan, *Appl. Catal., B*, 2008, **79**, 72–80.
- 9 N. Luo, Z. Jiang, H. Shi, F. Cao, T. Xiao and P. P. Edwards, *Int. J. Hydrogen Energy*, 2009, **34**, 125.
- 10 C. D. Valentin, E. Finazzi, G. Pacchioni, A. Selloni, S. Livraghi, A. M. Czoska, M. C. Paganini and E. Giamello, *Chem. Mater.*, 2008, **20**, 3706.
- 11 D. Li, H. Haneda, S. Hishita and N. Ohashi, *Chem. Mater.*, 2005, **17**, 2588–2595.
- 12 R. Asahi, T. Morikawa, T. Ohwaki, K. Aoki and Y. Taga, *Science*, 2001, **293**, 269.
- 13 Z. Jiang, F. Yang, N. Luo, B. T. T. Chu, D. Sun, H. Shi, T. Xiao and P. P. Edwards, *Chem. Commun.*, 2008, 6372–6374.
- 14 X. Chen, X. Wang, Y. Hou, J. Huang, L. Wu and X. Fu, *J. Catal.*, 2008, **255**, 59–67.
- 15 (a) M. Bellardita, M. Addamo, A. D. Paola, L. Palmisano and A. M. Venezia, *Phys. Chem. Chem. Phys.*, 2009, **11**, 4084–4093; (b) S. Yin, K. Ihara, Y. Aita, M. Komatsu and T. Sato, *J. Photochem. Photobiol., A*, 2006, **179**, 105–114.
- 16 A. Ghicov, J. M. Macak, H. Tsuchiya, J. Kunze, V. Haeublein, L. Frey and P. Schmuki, *Nano Lett.*, 2006, **6**, 1080.
- 17 K. S. Yang, Y. Dai and B. B. Huang, *J. Phys. Chem. C*, 2007, **111**, 12086.
- 18 J. M. Mwabora, T. Lindgren, E. Avendano, T. F. Jaramillo, J. Lu, S. E. Lindquist and C. G. Granqvist, *J. Phys. Chem. B*, 2004, **108**, 20193–20198.
- 19 I. C. Kang, Q. Zhang, S. Yin, T. Sato and F. Saito, *Appl. Catal., B*, 2008, **84**, 570.
- 20 Y. Yokosuka, K. Oki, H. Nishikiori, Y. Tatsumi, N. Tanaka and T. Fujii, *Res. Chem. Intermed.*, 2009, **35**, 43–53.
- 21 Q. Li, Y. W. Li, P. Wu, R. Xie and J. K. Shang, *Adv. Mater.*, 2008, **20**, 3717.
- 22 (a) S. Yin, Y. Aita, M. Komatsu, J. Wang, Q. Tang and T. Sato, *J. Mater. Chem.*, 2005, **15**, 674–682; (b) S. Yin, Y. Aita, M. Komatsu and T. Sato, *J. Eur. Ceram. Soc.*, 2006, **26**, 2735–2742; (c) Y. Aita, M. Komatsu, S. Yin and T. Sato, *J. Solid State Chem.*, 2004, **177**, 3235–3238; (d) L. Liu, W. Qin, S. Zuo, Y. Yu and Z. Hao, *J. Hazard. Mater.*, 2009, **163**, 273–278.
- 23 Z. Wu, F. Dong, W. Zhao and S. Guo, *J. Hazard. Mater.*, 2008, **157**, 57.
- 24 N. C. Saha and H. G. Tompkins, *J. Appl. Phys.*, 1992, **72**, 3072–3079.
- 25 F. Dong, W. Zhao and Z. Wu, *Nanotechnology*, 2008, **19**, 365607.
- 26 J. A. Rengifo-Herrera, K. Pierzchala, A. Sienkiewicz, L. Forro, J. Kivi and C. Pulgarin, *Appl. Catal., B*, 2009, **88**, 398–406.
- 27 H. Irie, Y. Watanabe and K. Hashimoto, *J. Phys. Chem. B*, 2003, **107**, 5483.
- 28 S. Livraghi, M. C. Paganini, E. Giamello, A. Selloni, C. D. Valentin and G. Pacchioni, *J. Am. Chem. Soc.*, 2006, **128**, 15666.

-
- 29 T. Xiao and Z. Jiang, *UK Patent*, WO 2008/009919 A1, 2008.
- 30 Y. Shen, T. Xiong, T. Li and K. Yang, *Appl. Catal., B*, 2008, **83**, 177–185.
- 31 W. Han, P. Liu, R. Yuan, J. Wang, Z. Li, J. Zhuang and X. Fu, *J. Mater. Chem.*, 2009, **19**, 6888–6895.
- 32 M. Mrowetz, W. Balcerski, J. Colussi and M. R. Hoffmann, *J. Phys. Chem. B*, 2004, **108**, 17269–17273.
- 33 J. Ananpattarachai, P. Kajitvichyanukul and S. Seraphin, *J. Hazard. Mater.*, 2009, **168**, 253–261.
- 34 J. Wang, W. Zhu, Y. Zhang and S. Liu, *J. Phys. Chem. C*, 2007, **111**, 1010.
- 35 Y. Sheng, Y. Xu, D. Jiang, L. Liang, D. Wu and Y. Sun, *Int. J. Photoenergy*, 2008, **2008**, 1.
- 36 K. Nagaveni, M. S. Hegde, N. Ravishankar, G. N. Subbanna and G. Madras, *Langmuir*, 2004, **20**, 2900.
- 37 D. Huang, S. Liao, S. Quan, L. Liu, Z. He, J. Wan and W. Zhou, *J. Mater. Res.*, 2007, **22**, 2389–2397.
- 38 J. Geng, D. Yang, J. Zhu, D. Chen and Z. Jiang, *Mater. Res. Bull.*, 2009, **44**, 146–150.
- 39 M. Primet, P. Pichat and M.-V. Mathieu, *J. Phys. Chem.*, 1971, **75**, 1216.
- 40 K. L. Yeung, S. T. Yau, A. J. Maira, J. M. Coronado, J. Soria and P. L. Yue, *J. Catal.*, 2003, **219**, 107.
- 41 Y. Huo, Y. Jin, J. Zhu and H. Li, *Appl. Catal., B*, 2009, **89**, 543–550.
- 42 K. Yanagisawa and J. Ovenstone, *J. Phys. Chem. B*, 1999, **103**, 7781–7787.
- 43 K. L. Frindell, M. H. Bartl, A. Popitsch and G. D. Stucky, *Angew. Chem., Int. Ed.*, 2002, **41**, 959–962.
- 44 K. R. Zhu, M. S. Zhang, Q. Chen and Z. Yin, *Phys. Lett. A*, 2005, **340**, 220.
- 45 H. M. Liu, W. S. Yang, Y. Ma, Y. A. Cao, J. N. Yao, J. Zhang and T. D. Hu, *Langmuir*, 2003, **19**, 3001.
- 46 E. A. Reyes-Garcia, Y. Sun, K. R. Reyes-Gil and D. Raftery, *Solid State Nucl. Magn. Reson.*, 2009, **35**, 74–81.
- 47 E. Serwicka, *Colloids Surf.*, 1985, **13**, 287.
- 48 S.-k. Joung, T. Amemiya, M. Murabayashi and K. Itoh, *Chem.–Eur. J.*, 2006, **12**, 5526.
- 49 J. M. Coronado, A. J. Maira, J. C. Conesa, K. L. Yeung, V. Augugliaro and J. Soria, *Langmuir*, 2001, **17**, 5368.
- 50 N. M. Dimitrijevic, Z. V. Sapomjic, B. M. Rabatic, O. G. Poluektov and T. Rajh, *J. Phys. Chem. C*, 2007, **111**, 14597.
- 51 G. Yang, Z. Jiang, H. Shi, M. O. Jones, T. Xiao, P. P. Edwards and Z. Yan, *Appl. Catal., B*, 2010, **96**, 458.
- 52 D. C. Hurum, A. G. Agrios, K. A. Gray, T. Rajh and M. C. Thurnauer, *J. Phys. Chem. B*, 2003, **107**, 4545.
- 53 H. Noda, K. Oikawa, T. Ogata, K. Matsuki and H. Kamata, *Chem. Soc. Jpn.*, 1986, **8**, 1084.